# NOTES AND CORRESPONDENCE

## The Liquid Water Oscillation in Modeling Boundary Layer Cumuli with Third-Order Turbulence Closure Models

Anning Cheng

*Atmospheric Sciences, NASA Langley Research Center, and Center for Atmospheric Sciences, Hampton University, Hampton, Virginia*

Kuan-Man Xu

*Atmospheric Sciences, NASA Langley Research Center, Hampton, Virginia*

Jean-Christophe Golaz

*National Research Council, Naval Research Laboratory, Monterey, California*

28 February 2003 and 2 January 2004

### ABSTRACT

A hierarchy of third-order turbulence closure models are used to simulate boundary layer cumuli in this study. An unrealistically strong liquid water oscillation (LWO) is found in the fully prognostic model, which predicts all third moments. The LWO propagates from cloud base to cloud top with a speed of $1 \text{ m s}^{-1}$. The period of the oscillation is about 1000 s. Liquid water buoyancy (LWB) terms in the third-moment equations contribute to the LWO. The LWO mainly affects the vertical profiles of cloud fraction, mean liquid water mixing ratio, and the fluxes of liquid water potential temperature and total water, but has less impact on the vertical profiles of other second and third moments.

In order to minimize the LWO, a moderately large diffusion coefficient and a large turbulent dissipation at its originating level are needed. However, this approach distorts the vertical distributions of cloud fraction and liquid water mixing ratio. A better approach is to parameterize LWB more reasonably. A minimally prognostic model, which diagnoses all third moments except for the vertical velocity, is shown to produce better results, compared to a fully prognostic model.

## 1. Introduction

Third-order turbulence closure (e.g., André et al. 1976; Bougeault 1981a,b; Krueger 1988) with a turbulence-scale condensation scheme (e.g., Sommeria and Deardorff 1977) is one of the approaches that researchers have used to parameterize the planetary boundary layer (PBL) clouds. Here, a third-order closure (TOC) model refers to a numerical model, which predicts some or all third moments and parameterizes the fourth moments using a closure assumption. A minimally prognostic TOC model diagnoses all third moments except for vertical velocity. Two examples are the higher-order closure model developed by Lappen and Randall (2001), which unifies the higher-order closure with the mass flux closure, and the model developed by Golaz et al. (2002a,b), which uses a double-Gaussian joint proba-

*Corresponding author address:* Dr. Anning Cheng, NASA Langley Research Center, Mail Stop 420, Hampton, VA 23681.
E-mail: a.cheng@larc.nasa.gov

bility density function (PDF) as basis for the closure. A fully prognostic TOC model, as its name implies, predicts all third moments.

Though there have been many successful applications of TOC models [cloud-resolving models (CRMs) or single-column models (SCMs)] in simulating the PBL, difficulties persist. The presence of spurious oscillation is one of them. There is spuriously wavelike behavior in the pollutant profiles of Deardorff's (1978) TOC model. He found that a diffusion coefficient proportional to the turbulent kinetic energy (TKE) is needed to damp such spurious oscillations. Using a 1D TOC model, Bougeault (1981a,b) identified a "spurious" oscillation in the vertical profiles of the second and third moments for shallow cumuli. An unrealistic oscillation in cloud fraction and liquid water flux was discussed by Wang and Wang (1994) in studying the effects of heavy drizzle on a nocturnal stratus-topped PBL. They suspected that the quasi-Gaussian closure assumption (Millionshchikov 1941), which expresses the fourth moments in terms

TABLE 1. A description of numerical experiments performed in this study.

| Expt | TOC model | Neglecting $q_l$ buoyancy | $K$ | Modified length scale | Closure |
|---|---|---|---|---|---|
| 1 (MP) | Minimally prognostic | N | 15 | N | Double Gaussian |
| 2 | Fully prognostic | N | 15 | N | Quasi Gaussian |
| 3 | Fully prognostic | Y | 15 | N | Quasi Gaussian |
| 4 | Fully prognostic | N | 30 | N | Quasi Gaussian |
| 5 | Fully prognostic | N | 30 | Y | Quasi Gaussian |

of the second moments assuming that the variables have a Gaussian distribution, is not consistent with the turbulence structure of the PBL with high skewness.

Moeng and Randall (1984, hereafter MR) examined a spurious oscillation in TOC modeling of stratocumulus clouds. This oscillation cannot be found in observational data and large-eddy simulations (LESs); that is why they labeled it spurious. They found that the spurious oscillation is located near the cloud top where the thermal radiative cooling and the mean gradients of temperature and moisture are the largest. They obtained a ''wave equation'' by combining two equations containing the buoyancy and the mean gradient terms. The period of the oscillation is 100 s. They found that choosing a larger diffusion coefficient can effectively damp the oscillation in the dry-cloud case, but a larger dissipation coefficient is needed to weaken the spurious oscillation in the wet-cloud case. Bougeault and André (1986) later suggested that a better formulation of the turbulent length scale be used to dampen the spurious oscillation.

It is very important to identify and investigate various oscillations in order to produce reasonable results from TOC models. The objective of this paper is to report one such oscillation, the liquid water oscillation (LWO), in fully prognostic TOC models and discuss several methods to weaken it.

## 2. Model description and experiment design

The National Aeronautics and Space Administration (NASA) Langley Research Center two-dimensional (LaRC-a) CRM, which is better known as the University of California, Los Angeles (UCLA)/Colorado State University (CSU) CRM (Krueger 1988; Xu and Randall 1995), is used in this study. It was extensively used at CSU by the second author in the 1990s and evaluated by simulating tropical and midlatitude deep convection (Xu and Randall 1996, 2000). An important feature of this CRM is its fully prognostic TOC. A major addition to the model is that a minimally prognostic TOC has been implemented and tested in this model, following Golaz et al. (2002a), so that a comparison of the different levels of complexity of TOC models becomes possible.

The LaRC-a model is run in 1D, and the Barbados Oceanographic and Meteorological Experiment (BOMEX) case is chosen to study the LWO in shallow cumuli since this case has been extensively simulated by LESs (e.g., Siebesma et al. 2003). The results from 10 LESs (Siebesma et al. 2003) are available as a benchmark to compare with 1D simulations. The cloud fraction for this case is about 10%. It is a purely shallow cumulus case, with no transitions from/to or remnants of stratocumulus. The configuration of the LaRC-a model is the same as used in LESs. Please refer to Siebesma et al. (2003) for details.

Five experiments have been performed in this study. The design of these experiments is described in Table 1. Outputs from every 1 min are used to plot all figures. Experiment 1 uses minimally prognostic closure with smallest diffusion coefficient (hereafter, experiment MP). The results from experiment MP are comparable to those of Golaz et al. (2002b). Experiment 2 is used to demonstrate the presence of the LWO, with fully prognostic closure and smallest diffusion coefficient. The LWO is weakened in experiment 3 when the liquid water buoyancy (LWB) terms[1] in the third-moment equations are neglected. By comparing the results of 10 LESs [see Siebesma et al. (2003) for details of these LESs] with experiments MP, 2, and 3, we attempt to investigate the mechanism that causes the LWO. We use a larger diffusion coefficient to damp the LWO in experiment 4 and both a larger diffusion coefficient and a larger dissipation coefficient to weaken the LWO in experiment 5. Results from experiments 4 and 5, as shown later, are comparable to those of other fully prognostic models, such as Bougeault (1981a,b) and Krueger and Bergeron (1994).

## 3. Liquid water oscillation

Before investigating the LWO in the fully prognostic TOC model, we need to have some idea on the results by LESs and the minimally prognostic model. Figures 1a and 1b show the time–height cross section of cloud fraction from the Regional Atmospheric Modeling System (RAMS) LES (from Golaz 2001) and experiment MP, respectively. There are some temporal fluctuations of cloud fraction in LES after an initial burst of convection at hour 1. The LES produces the maximum cloud fraction near the cloud base. The cloud fraction decreases with height. This is because most of the shal-

---

[1] Here, $\overline{u_i' a' q_l'}$, $\overline{u_i' u_j' q_l'}$, and $\overline{a' b' q_l'}$ are defined as the LWB terms, where $u_i$ and $u_j$ can be $u$, $v$, or $w$, and $a$ and $b$ can be $\theta_l$ or $q_t$, liquid water potential temperature and total water mixing ratio, since they appear in the buoyancy terms of third-moment equations and are related to liquid water mixing ratio inside clouds.
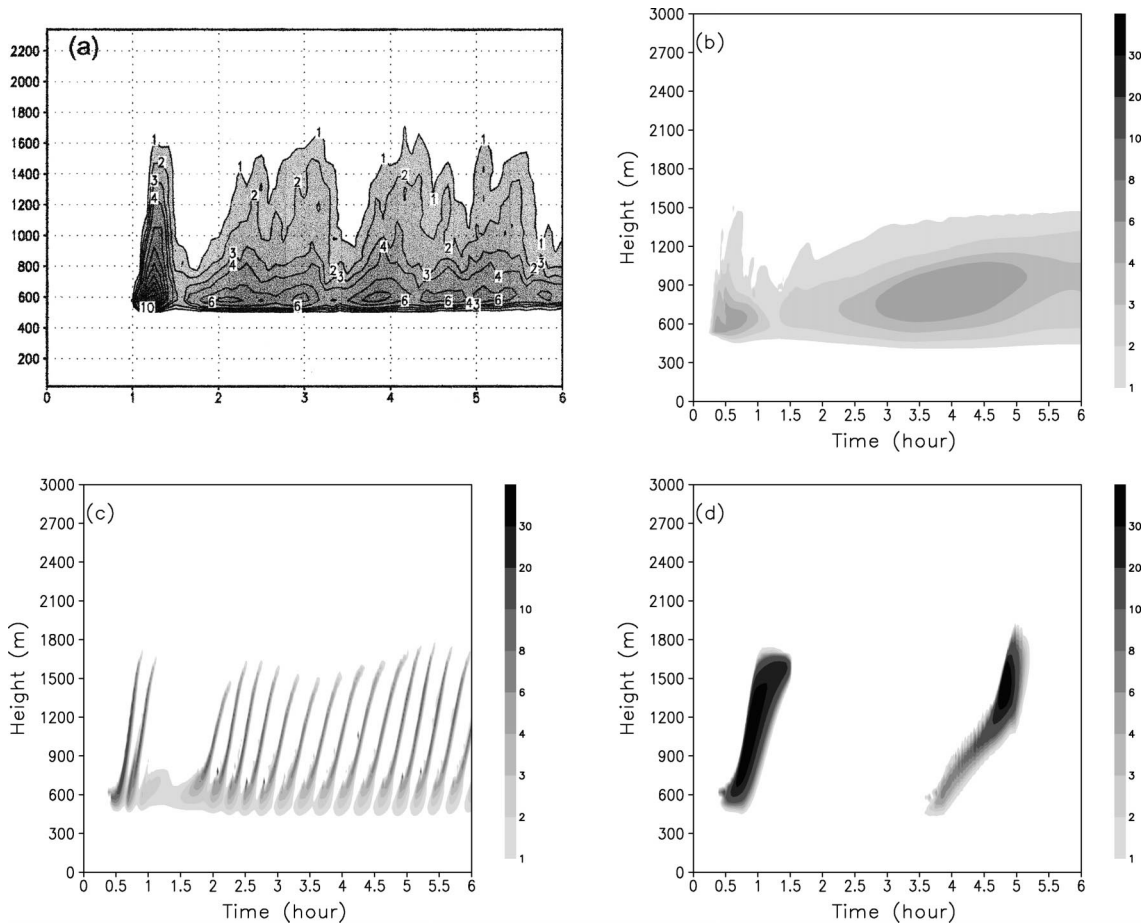
FIG. 1. Time series of cloud fractions for BOMEX from (a) RAMS LES, (b) expt MP (expt 1), (c) expt 2, and (d) expt 3. Expt MP is the basic experiment from the minimally prognostic model. Expt 2 uses the fully prognostic model with the least diffusion coefficient, while expt 3 neglects the LWB terms.

low cumuli cannot reach the domain-maximum cloud top. The temporal evolution of cloud fraction from experiment MP is more steady than the LES. The maximum cloud fraction moves to the middle of the layer at the end of integration. It seems that there is still some room for improvement of the results presented in experiment MP. However, it is the best result that we can find among the current 1D TOC models (see Lappen and Randall 2001; Golaz et al. 2002b).

The oscillation is obvious in experiment 2 (Fig. 1c), but such an oscillation is not apparent in either the LESs or experiment MP. For any given time in Fig. 1c, we can see a few cloud events. A cloud event refers to a burst of clouds growing from 600 to 1800 m and then dying out. The cloud events at a higher altitude are in a mature stage and have a larger cloud fraction, while the cloud events at a lower altitude are in a developing stage and have a smaller cloud fraction. Here, the period of the oscillation is about 15 min. The oscillation propagates upward with a phase speed of 1 m s$^{-1}$.

The LWO has a close relationship with LWB terms in the third-moment equations, such as $\overline{u_i'a'q_l'}$, $\overline{u_i'u_j'q_l'}$,

and $\overline{a'b'q_l'}$. Figure 1d shows the result from experiment 3 when these terms are set equal to zero only in the third-moment equations. There is no obvious temporal oscillation since the two cumulus events are not similar to each other. It should be emphasized that only liquid-water-related buoyancy is neglected in the third-moment equations. The thermal buoyancy is still produced. The LWB is still present in the first- and second-moment equations and condensation is still computed. So, this experiment is more realistic than a dry run (e.g., MR), which completely neglects the effects of liquid water and condensation. Thus, this experiment reveals the cause of the LWO. Another important conclusion drawn from Fig. 1d is that the LWO is not associated with $\overline{\theta_l'^3}$, $\overline{\theta_l'^2 q_w'}$, $\overline{\theta_l' q_w'^2}$, and $\overline{q_t'^3}$ equations because there are no buoyancy production terms in these equations.

Based upon these three experiments, it is obvious that LWB in the third-moment equations plays an important role in the LWO. This is a basic difference between the LWO and the spurious oscillation of MR. Further mathematical derivation is given below.

From the $\overline{w'^3}$ equation,

$$\left(\frac{\partial}{\partial t} + \overline{w}\frac{\partial}{\partial z}\right)\overline{w'^3} = \frac{3g}{\overline{T}}\left\{\left[\frac{p_0}{p_r(z)}\right]^k\frac{L}{c_p} - 1.61\overline{T}\right\}\overline{w'w'q_l'}$$
$$+ \text{ other terms,} \quad (1)$$

where the prime stands for perturbation from the ensemble mean; $\overline{w}$ and $\overline{T}$ are the mean vertical velocity and the mean temperature, respectively; $p_0$ is the reference pressure $10^5$ Pa; $p_r(z)$ is the mean pressure at height $z$; $L$ is the latent heat of vaporization; $k = c_p/R_d$, $R_d$ is the gas constant for dry air; and $c_p$ is the specific heat at constant pressure of dry air. Based on an LES solution, Bougeault (1981a; his Fig. 16) related $\overline{w'w'q_l'}$ and $\overline{w'w's'}$ as the following:

$$\overline{w'w'q_l'} = \frac{2\overline{w'w's'}}{r_{wws}}(Q_1^2 - 4Q_1 + 5)\exp(Q_1 - 1), \quad (2)$$

where $r_{wws}$ is the correlation between $w'^2$ and $s'$, $Q_1$ is a dimensionless measure of the departure of the mean state from saturation, $Q_1 = \alpha[(\overline{q_t} - \overline{q_{sl}})/2\sigma_s]$, and $s' = (\alpha/2)(q_t' - \alpha_1\theta_l')$ (Mellor 1977), where $\sigma_s$ represents variance of $s$, $\alpha = (1 + L^2\overline{q_{sl}}/R_v c_p \overline{T_l^2})^{-1}$, and $\alpha_1 = \overline{q_{sl}}(L/R_v\overline{T_l^2})(\overline{T}/\theta)$. We also define $\overline{s} = (\alpha/2)(\overline{q_t} - \alpha_1\overline{\theta_l})$. Equation (2) is based on an empirical skewed distribution of liquid water potential temperature and total water. Applying $(\partial/\partial t + \overline{w}(\partial/\partial z))$ to (1) and (2), and using the relationship of $\overline{w'w's'} = (\alpha/2)(\overline{w'w'q_t'} - \alpha_1\overline{w'w'\theta_l'})$ and the predictive equations of $\overline{w'w'q_t'}$ and $\overline{w'w'\theta_l'}$, we have

$$\left(\frac{\partial}{\partial t} + \overline{w}\frac{\partial}{\partial z}\right)^2\overline{w'^3} = -N^2\overline{w'^3} + \text{ other terms,} \quad (3)$$

where $N^2 = (3g\alpha/\overline{T}r_{wws})[(p_0/p_r(z))^k(L/c_p) - 1.61\overline{T}]$ $(\partial\overline{s}/\partial z)(Q_1^2 - 4Q_1 + 5)\exp(Q_1 - 1)$.

The dispersion relationship can be found:

$$\omega = \overline{w}m \pm N, \quad (4)$$

where $m$ is the wavenumber in the vertical direction. The phase speed of the oscillation is

$$v_p = \overline{w} \pm N/m. \quad (5)$$

### a. Cloud fraction and $\overline{w'^3}$

The wave equation (3) is for $\overline{w'^3}$, which is the third moment of vertical velocity, but the oscillation shown in Fig. 1c is in the cloud fraction. How does the oscillation in the third moment of vertical velocity influence the cloud fraction?

A link between updraft area and the skewness ($sk_w = \overline{w'^3}/\overline{w'w'}^{3/2}$) of vertical velocity (Randall et al. 1992; Lappen and Randall 2001) can be expressed by

$$a = \frac{1}{2}\left[1 - sk_w\left(\frac{1}{4 + sk_w^2}\right)^{-1/2}\right], \quad (6)$$

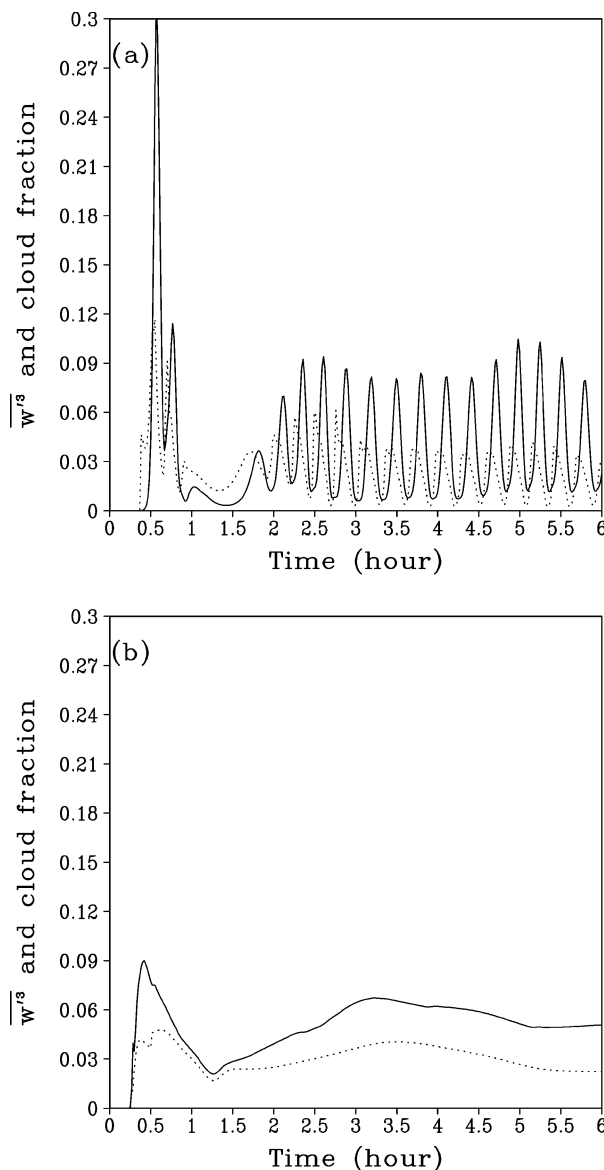where $a$ is the updraft-area fraction. A more sophisticated formula can be found in Golaz et al. (2002a).



FIG. 2. Time series of the third moment of vertical velocity (solid line) and cloud fraction (dotted line) at 620 m from (a) expt 2, and (b) expt MP.

When $sk_w = 0$, $a = 0.5$, the updrafts and downdrafts have the same fraction. From (6), when the skewness increases, the updraft-area fraction decreases. Shallow cumuli usually have a skewness of about 3. Cloud is produced in the updrafts. So (6) establishes a close relationship between $\overline{w'^3}$ and the cloud fraction. It should be emphasized that this relationship is based on a simple probability distribution function (PDF) used by Lappen and Randall (2001). In addition to skewness, many other factors such as the distributions of moisture, temperature, and pressure also influence the condensation, and thus the cloud fraction.

Figure 2 shows the time series of $\overline{w'^3}$ and the cloud fraction at 620 m for experiments MP and 2. The cloud
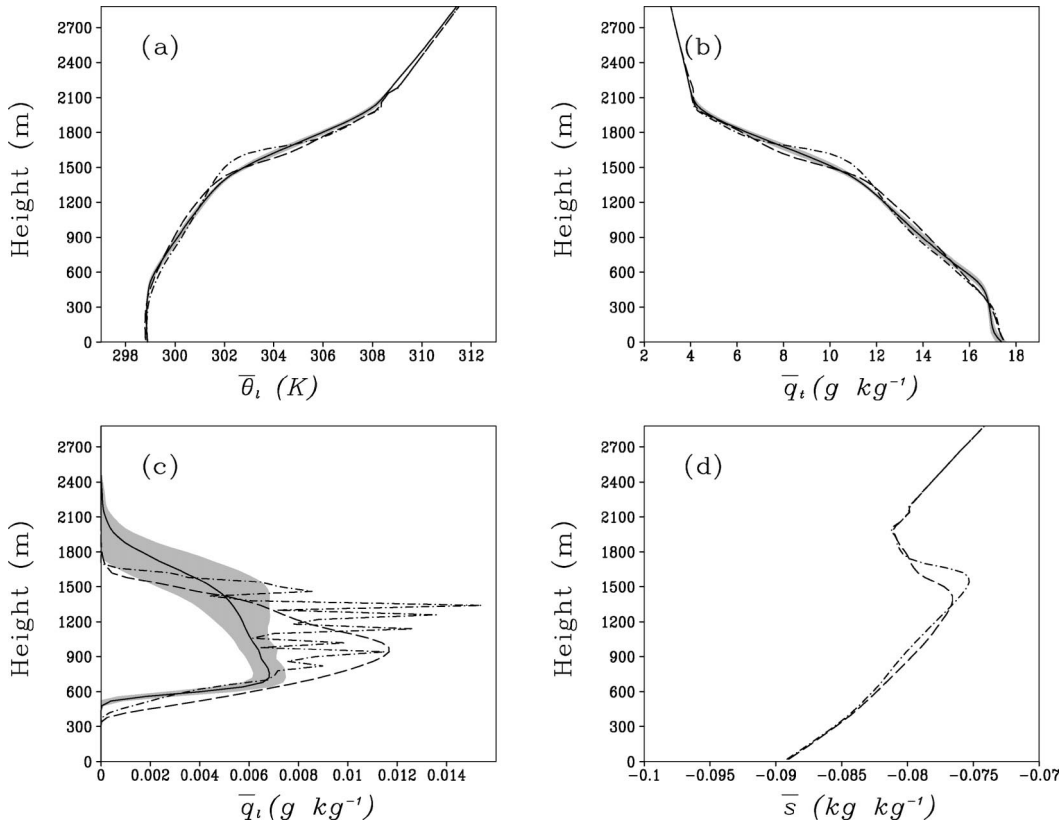
FIG. 3. Mean profiles averaged from $t = 4$ h to $t = 5$ h of (a) liquid potential temperature, (b) total water specific humidity, (c) liquid water mixing ratio, and (d) $\overline{s}$. The solid lines indicate the LES average, and the shaded band has a width of twice the standard deviation of the LESs. The long-dashed line is for expt MP, and the dashed–dotted line is for expt 2.

fraction and $\overline{w'^3}$ are positively correlated in experiments MP and 2. This is because the mean state is unsaturated near the cloud-base level. A large value of $\overline{w'^3}$ is needed to produce a small updraft-area fraction.

From the above analysis, we find that the oscillation in $\overline{w'^3}$ can cause the oscillation in the cloud fraction since they are related by (6). But how does the cloud fraction affect the higher moments? In the fully prognostic TOC model, cloud fraction and condensation are related by the turbulence-scale condensation scheme

$$\overline{q_l} = a\overline{q_{l1}} + (1 - a)\overline{q_{l2}}, \tag{7}$$

where $\overline{q_l}$ is the mean liquid water mixing ratio; subscripts 1 and 2 refer to the first and second Gaussians, respectively; and $\overline{q_{li}} = \overline{s_i}C_i + \sigma_{si}/\sqrt{2\pi}\,\exp[-(1/2)(\overline{s_i}/\sigma_{si})^2]$, where $i$ can be 1 or 2. The condensation alters the buoyancy production in the second- and third-moment equations. The latent heat released by condensation also increases the mean temperature and decreases the mean water vapor mixing ratio. The second moments, such as the vertical fluxes of liquid potential temperature and total water, are related to the gradient of the first moments. The third moments can also be influenced by the second moments and the first moments

through the mean gradient terms[2] and turbulent advection terms.

### b. Propagation mechanism

From Eq. (5), we can estimate the phase speed of the oscillation. The profile of $\overline{s}$ is plotted in Fig. 3d. From this figure, we can see that $\partial\overline{s}/\partial z$ is positive below 1500 m and above 1800 m. So, the oscillation cannot be produced between 1500 and 1800 m since $N^2$ is negative when $\partial\overline{s}/\partial z$ is negative. We can estimate $\partial\overline{s}/\partial z \sim 10^{-5}$ m$^{-1}$, $(3g/T_0)[(p_0/p_r(z))^k(L/c_p) - 1.61T_0] \approx 200$ m s$^{-2}$, $Q_1 = -4$, $\alpha = 0.3$, and $r_{wws} \sim 1$ near cloud base. This leads to $N^2 \sim 10^{-6}$ s$^{-2}$. From Fig. 1c, we find that there is no vertical variation of each cloud cycle, so a single wave fills the cloud layer. The wavelength is about 1000 m, and the wavenumber ($m$) of the oscillation is in the order of 0.001 m$^{-1}$. From (4), the period is about 1000 s, and using (5) the phase speed is approximately $\pm 1$ m s$^{-1}$. The period and the magnitude of the phase

---

[2] As defined by Moeng and Randall (1984), the mean gradient terms include $\partial\overline{u_i}/\partial z$ or $\partial\overline{a}/\partial z$, where $u_i$ can be $u$, $v$, or $w$, and $a$ can be $\theta_l$ or $q_t$.
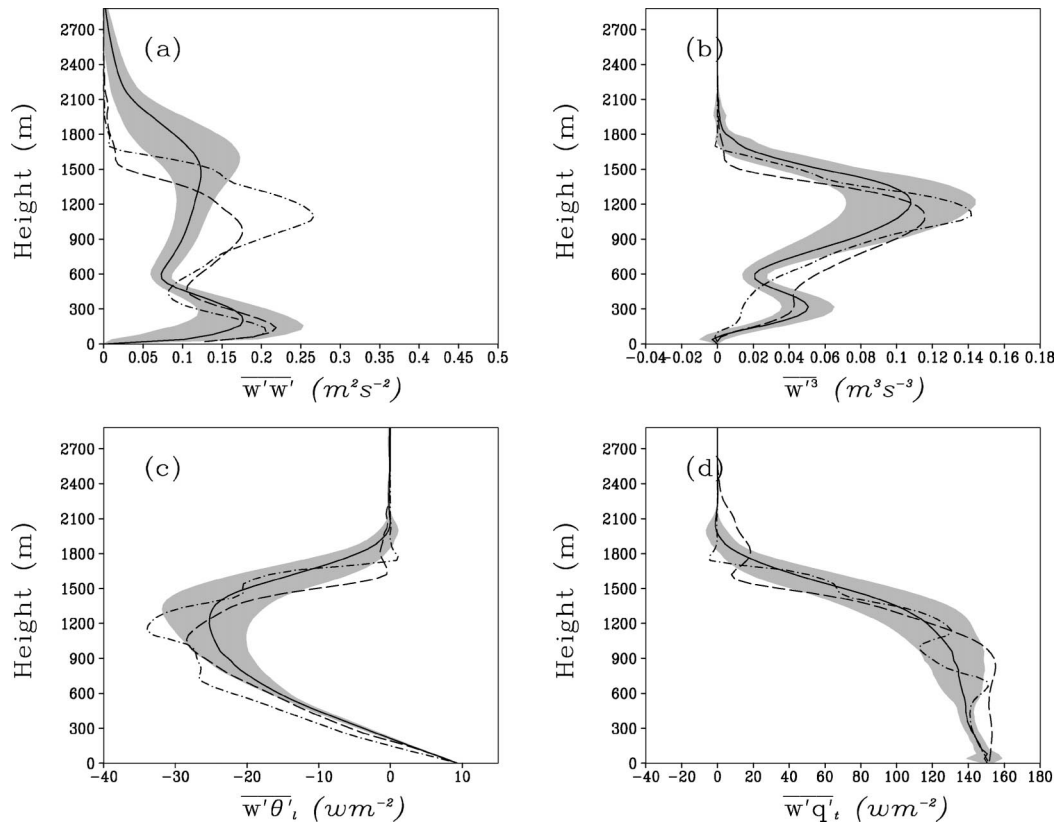
FIG. 4. Profiles of (a) $\overline{w'^2}$, (b) $\overline{w'^3}$, (c) $\overline{w'\theta_l'}$, and (d) $\overline{w'q_t'}$ averaged from $t = 4$ h to $t = 5$ h. The solid lines indicate the LES average, and the shaded band has a width of twice the standard deviation of the LESs. The long-dashed line represents expt MP, and the dashed–dotted line represents expt 2.

speed compares well with those from Fig. 1c. However, the oscillation only propagates upward. This may be due to the fact that the fluxes of total water and liquid water potential temperature are upward. Another reason is that $Q_1$ increases with height. It can be equal to 1 near cloud top. A large value of $Q_1$ leads to an exponential increase of $N^2$, which means that the frequency of the oscillation near the cloud top is higher and the wavelength is shorter. This high-frequency oscillation can be damped with the smaller diffusion coefficient used in the TOC model and cannot propagate downward. The spurious oscillation of MR originates from the strong inversion layer and propagates downward.

### c. Vertical structure

In order to obtain a better understanding of the LWO, the vertical structure of the first moments, the second moments, and the third moment of vertical velocity are discussed in this section. We choose hourly averaged profiles at hour 5 because the LESs and experiment MP are near a steady-state regime at this time. We can also find the impact of the LWO on the simulation by comparing the results from the LESs and experiments MP and 2.

Figures 3a and 3b show the profiles of liquid water potential temperature ($\overline{\theta}_l$) and total water ($\overline{q}_t$), respectively. There are no oscillations in these two profiles. Profiles from experiment 2 are similar to those of experiment MP in the subcloud layer and the cloud layer, but experiment 2 produces a stronger stable layer near the cloud top (moister and colder) than the LESs and experiment MP. This mixing process may be due to large cloud-top entrainment caused by the LWO.

We can see several oscillations in $\overline{q}_l$ profile from experiment 2 (Fig. 3c). These oscillations are associated with the LWO. We will show that such oscillations disappear when the LWO is eliminated. The LWO influences the profile of the first moment $\overline{q}_l$, but the spurious oscillation of MR only affects the higher moments. Experiment MP produces larger $\overline{q}_l$ near the cloud base than the LESs. This is what we expected, because the diagnostic $\overline{q}_l$ from the double-Gaussian distribution tends to be larger (see Golaz et al. 2002b).

There are oscillations in the profiles of $\overline{w'\theta_l'}$ and $\overline{w'q_t'}$ (Figs. 4c and 4d), but no oscillations in $\overline{w'^2}$ and $\overline{w'^3}$ (Figs. 4a and 4b). These oscillations are also associated with the LWO. In the model, the formulas of $\overline{\theta_l'q_t'} = C\theta_l's'$ and $\overline{q_t'q_t'} = Cq_t's'$, are used to calculate the buoyancy for prognostic equations of $\overline{w'\theta_l'}$ and

$\overline{w'q'_t}$. So, oscillations in cloud fraction ($C$) can result in oscillations in the vertical fluxes. Despite the presence of LWO, the vertical profiles of $\overline{w'\theta'_l}$ and $\overline{w'q'_t}$ from experiment 2 compare well with experiment MP and the LESs.

In summary, the LWO is mainly caused by the interaction of the LWB and the mean gradient of $\overline{s}$ in the third-moment equations, where $\overline{s}$ is a linear function of $\overline{\theta}_l$ and $\overline{q}_t$, which means the LWO is related to both $\overline{\theta}_l$ and $\overline{q}_t$. The LWO propagates upward and has an impact on the cloud fraction and the mean liquid water mixing ratio. The second moments are also influenced. In the rest of this paper, we will discuss some methods used to weaken the LWO and their unexpected effects on the vertical distributions of the simulated clouds.

## 4. Methods to weaken the LWO

### a. Diffusion

Diffusion of any moment $\chi$ can be expressed by

$$K\nabla^2\chi, \tag{8}$$

where $K$ is the diffusion coefficient, and $\nabla^2 = \partial^2/\partial x^2 + \partial^2/\partial y^2 + \partial^2/\partial z^2$. Figure 5a shows the time–height cross section of cloud fraction for experiment 4. The values of $K$ are 2 times larger than that in experiment 2. Comparing Fig. 5a with Fig. 1c, it is found that short-period LWOs have been eliminated. However, there are still some oscillations in the vertical direction at 1, 2, 4, and 6 h in Fig. 5a. This long-period oscillation is similar to the oscillation reported by Wang and Wang (1994). The intermittent behavior shown in Fig. 5a suggests that the turbulence is not in balance with the imposed large-scale forcing. The vertical distribution of the cloud fraction is not reasonable, compared to Fig. 1a. Krueger and Bergeron (1994) also obtained a very similar profile of cloud fraction (their Fig. 1).

The mean profiles of $\overline{\theta}_l$ and $\overline{q}_t$ from experiment 4 are more strongly mixed than the LESs and experiment MP (not shown). The value of $\overline{q}_l$ is smaller (Fig. 6) than that shown in Fig. 3c. Furthermore, its vertical distribution is not reasonable: $\overline{q}_l$ near the cloud base is much smaller than that produced by the LESs. Bougeault (1981b) used a TOC model to simulate a shallow cumulus case. He also obtained a very similar $\overline{q}_l$ profile (his Fig. 8). He attributed it to the consequence of the parameterizations of the second and third moments.

### b. Turbulent dissipation

While diffusion is a process that spreads the oscillation energy, large turbulent dissipation can be used to damp the oscillation (MR; Bougeault and André 1986). A modified turbulent length scale (not shown) is proposed to understand to what extent turbulent dissipation can damp the oscillation. The modified turbulent length scale produces larger dissipation (doubled) at and below
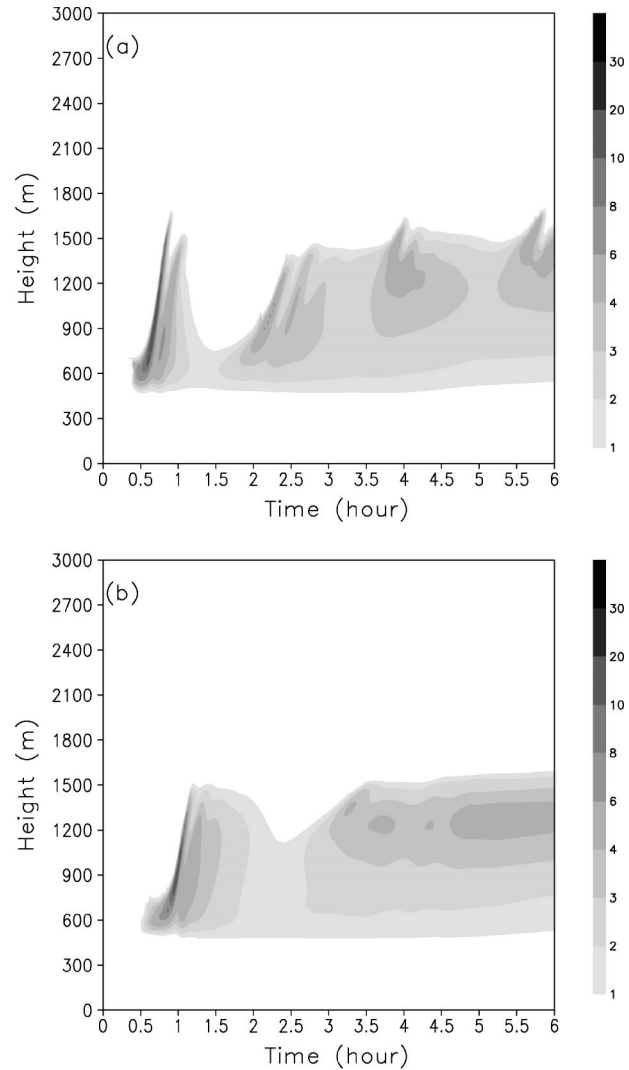


FIG. 5. Time series of cloud fractions from (a) expt 4 and (b) expt 5.

the originating level of the LWO. This approach does little to alter the profile of cloud fraction, especially the location of the maximum (Fig. 5b), which is distorted, as discussed earlier, when the diffusion coefficient is increased alone.

A positive impact of increasing dissipation is that the longer-period oscillation in experiment 4 (Fig. 5a) disappears near cloud top, although the dissipation near cloud base, not top, is doubled in experiment 5. By comparing Figs. 5a and 5b, we see that the main difference between experiments 4 and 5 occurs near cloud tops. The first, second, and third moments produced by experiment 5 have slightly smaller magnitudes than those with the larger diffusion only (not shown). Compared to the LESs and experiment MP, results from experiment 5 are still reasonable, except for vertical profiles of cloud fraction and cloud water mixing ratio (Fig. 6).
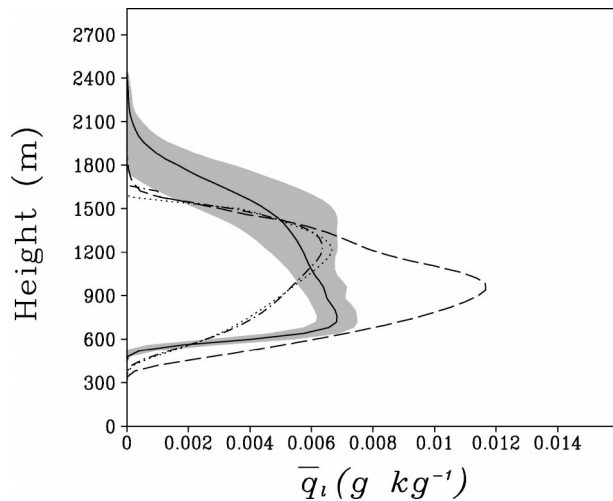
FIG. 6. Mean profiles averaged from $t = 4$ h to $t = 5$ h of liquid water mixing ratio. The solid lines indicate the LES average, and the shaded band has a width of twice the standard deviation of the LESs. The long-dashed line represents expt MP, the dashed–dotted line represents expt 4, and the dotted line represents expt 5.
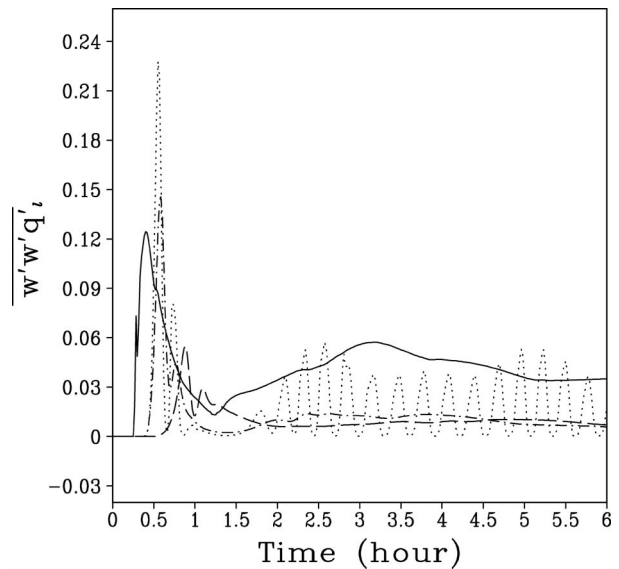


FIG. 7. Time series of LWB $(\overline{w'w'q_l'})$ at 620 m: the solid line represents expt MP, the dotted line represents expt 2, the dashed–dotted line represents expt 4, and the long-dashed line represents expt 5.

## c. Parameterization of the liquid water buoyancy

As discussed earlier, the physical mechanism of the LWO is related to the interaction of $\partial \overline{s}/\partial z$ with the LWB terms in the third-moment equations. The $\partial \overline{s}/\partial z$ terms from experiments MP, 2, 3, 4, and 5 are very similar near the cloud base (Fig. 3d shows experiments MP and 2). So a better parameterization for the LWB as in Golaz (2001, A.14) is a solution. He diagnoses the LWB using a double-Gaussian-based distribution of $\overline{\theta}_l$, $\overline{q}_t$, and $w$ instead of (2). Figure 7 shows the LWB at level 620 m. The LWB from experiment 2 has a larger value, and is in a state of oscillation. The LWB from experiments 4 and 5 is much smaller than that of experiment MP. As we have shown before, the profile of $\overline{q}_l$ and time series of cloud fraction from experiment MP are more realistic than those with larger diffusion coefficient and/or dissipation.

## 5. Summary and discussion

A hierarchy of third-order turbulence closure models have been used to simulate boundary layer cumulus clouds in this study. An unrealistically strong LWO has been found in the fully prognostic TOC model. The LWO propagates from cloud base to cloud top with a speed of 1 m s$^{-1}$. The period of the oscillation is about 1000 s. LWB terms in the third-moment equations contribute to the LWO. The LWO mainly affects the vertical profiles of cloud fraction, mean liquid water mixing ratio, and the fluxes of liquid water potential temperature and total water, but has less impact on the vertical profiles of other second and third moments.

This oscillation is different from the "spurious" oscillation of Moeng and Randall (1984) in the origin,

phase speed, period, mechanism, and impact of moments. First of all, the LWO is evident in cloud fraction and mean liquid mixing ratio, while the spurious oscillation does not have much effect on the first moments. Second, the LWO originates near cloud base and propagates upward, while the spurious oscillation originates in the inversion layer near cloud top and propagates downward. Third, the period of spurious oscillation is about 100 s, which is much shorter than that of the LWO. Finally, the LWO is due to the interaction of the mean gradient of $\overline{s}$ with the LWB terms in the third-moment equations, while the spurious oscillation arises from the mean gradient and buoyancy terms of the third-moment equations.

This study has also compared three methods to weaken the LWO. One method is using a large diffusion coefficient. This method damps the LWO effectively. The vertical profiles of mean liquid water potential temperature, total water, the second moments, and the third moments are all reasonable compared to the LESs and experiment MP, but there are still some longer-period oscillations near cloud top. Another method is using both a larger diffusion coefficient and larger dissipation near the originating level of the LWO. The longer-period oscillation near the cloud top is eliminated using this method and the other moments have slightly smaller magnitudes than the first method due to the larger dissipation. These two approaches have a common problem: they produce unrealistic vertical distributions of cloud fraction and liquid water mixing ratio. A better method is to use an improved parameterization of the LWB terms in the third-moment equations as in experiment MP. This method basically corrects the problem

of the unrealistic vertical profile of cloud fraction and liquid water mixing ratio. The vertical profiles of the other moments are also reasonable with this method.

As we mentioned above, there is still room for improvements in the 1D TOC models. In the future, we will develop a new model, with the third moments of liquid potential temperature and the total water predicted instead of diagnosed as in the MP model. Such a model holds promise since it adds more prognostic third-moment equations that do not contain buoyancy terms. The issue of the LWO can be avoided and the computational cost will not increase much. The skewnesses of liquid potential temperature and the total water will potentially provide more information about subgrid scales.

## REFERENCES

André, J. C., G. De Moor, P. Lacarrère, and R. Du Vachat, 1976: Turbulence approximation for inhomogeneous flows. Part I: The clipping approximation. *J. Atmos. Sci.,* **33,** 476–481.

Bougeault, P., 1981a: Modeling the trade-wind cumulus boundary layer. Part I: Testing the ensemble cloud relations against numerical data. *J. Atmos. Sci.,* **38,** 2414–2428.

——, 1981b: Modeling the trade-wind cumulus boundary layer. Part II: A high-order one-dimensional model. *J. Atmos. Sci.,* **38,** 2429–2439.

——, and J.-C. André, 1986: On the stability of the third-order turbulence closure for the modeling of the stratocumulus-topped boundary layer. *J. Atmos. Sci.,* **43,** 1574–1581.

Deardorff, J. W., 1978: Closure of second and third-moment rate equations for diffusion in homogeneous turbulence. *Phys. Fluids,* **21,** 525–530.

Golaz, J.-C., 2001: A PDF-based parameterization for boundary layer clouds. Ph.D. dissertation, Department of Atmospheric Science, Colorado State University, 124 pp.

——, V. E. Larson, and W. R. Cotton, 2002a: A PDF-based model for boundary layer clouds. Part I: Method and model description. *J. Atmos. Sci.,* **59,** 3540–3551.

——, ——, and ——, 2002b: A PDF-based model for boundary layer clouds. Part II: Model results. *J. Atmos. Sci.,* **59,** 3552–3571.

Krueger, S. K., 1988: Numerical simulation of tropical cumulus clouds and their interaction with the subcloud layer. *J. Atmos. Sci.,* **45,** 2221–2250.

——, and A. Bergeron, 1994: Modeling the trade cumulus boundary layer. *Atmos. Res.,* **33,** 169–192.

Lappen, C.-L., and D. A. Randall, 2001: Toward a unified parameterization of the boundary layer and moist convection. Part I: A new type of mass-flux model. *J. Atmos. Sci.,* **58,** 2021–2036.

Mellor, G. L., 1977: The Gaussian cloud model relations. *J. Atmos. Sci.,* **34,** 356–358.

Millionshchikov, M., 1941: On the theory of homogeneous and isotropic turbulence. *C. R. Acad. Sci. USSR,* **32,** 615–618.

Moeng, C.-H., and D. A. Randall, 1984: Problems in simulating the stratocumulus-topped boundary layer with a third-order closure model. *J. Atmos. Sci.,* **41,** 1588–1600.

Randall, D. A., Q. Shao, and C.-H. Moeng, 1992: A second-order bulk boundary-layer model. *J. Atmos. Sci.,* **49,** 1903–1923.

Siebesma, A. P., and Coauthors, 2003: A large-eddy simulation intercomparison study of shallow cumulus convection. *J. Atmos. Sci.,* **60,** 1201–1219.

Sommeria, G., and J. W. Deardorff, 1977: Subgrid-scale condensation in models of nonprecipitating clouds. *J. Atmos. Sci.,* **34,** 344–355.

Wang, S., and Q. Wang, 1994: Roles of drizzle in a one-dimensional third-order turbulence closure model of the nocturnal stratus-topped marine boundary layer. *J. Atmos. Sci.,* **51,** 1559–1576.

Xu, K.-M., and D. A. Randall, 1995: Impact of interactive radiative transfer on the macroscopic behavior of cumulus ensembles. Part I: Radiation parameterization and sensitivity tests. *J. Atmos. Sci.,* **52,** 785–799.

——, and ——, 1996: Explicit simulation of cumulus ensemble with the GATE Phase III data: Comparison with observations. *J. Atmos. Sci.,* **53,** 3710–3736.

——, and ——, 2000: Explicit simulation of midlatitude cumulus ensembles: Comparison with ARM data. *J. Atmos. Sci.,* **57,** 2839–2858.